

# A Stability Diagram for Dense Suspensions of Model Colloidal $\text{Al}_2\text{O}_3$ -Particles in Shear Flow

Martin Hecht,<sup>1</sup> Jens Harting,<sup>1</sup> and Hans J. Herrmann<sup>2,3</sup>

<sup>1</sup>*Institute for Computational Physics, Pfaffenwaldring 27, 70569 Stuttgart, Germany*

<sup>2</sup>*Computational Physics, IFB, Schafmattstr. 6,*

*ETH Zürich, CH-8093 Zürich, Switzerland*

<sup>3</sup>*Departamento de Física, Universidade Federal do Ceará Campus do Pici, 60451-970 Fortaleza CE, Brazil*

(Dated: March 23, 2022)

**Abstract.** In  $\text{Al}_2\text{O}_3$  suspensions, depending on the experimental conditions very different microstructures can be found, comprising fluid like suspensions, a repulsive structure, and a clustered microstructure. For technical processing in ceramics, the knowledge of the microstructure is of importance, since it essentially determines the stability of a workpiece to be produced. To enlighten this topic, we investigate these suspensions under shear by means of simulations. We observe cluster formation on two different length scales: the distance of nearest neighbors and on the length scale of the system size. We find that the clustering behavior does not depend on the length scale of observation. If inter-particle interactions are not attractive the particles form layers in the shear flow. The results are summarized in a stability diagram.

PACS numbers: 82.70.-y, 47.11.-j, 02.70.Ns, 77.84.Nh

## I. INTRODUCTION

Colloid science is a very fascinating research field, gaining more and more importance in the last years. It closely connects physics, chemistry, material science, biology, and several branches of engineering technology. According to its key role in modern science a considerable amount of research has been performed to describe colloidal suspensions from a theoretical point of view and by simulations [1, 2, 3, 4, 5, 6] as well as to understand the particle-particle interactions [7, 8, 9, 10, 11, 12], the phase behavior [13, 14, 15, 16], the relevant processes on the microscale and their influence on macroscopic parameters [17, 18, 19]. Colloidal suspensions are in fact complicated systems, since different time and length scales are involved. The particle sizes are on a mesoscopic length scale, i.e., in the range of nanometers up to micrometers. In systems of particles sized on this length scale Brownian motion often cannot be neglected. Depending on the particle sizes, materials, and concentrations, different interactions are of relevance and often several of them are in a subtle interplay: electrostatic repulsion, depletion forces, van der Waals attraction, hydrodynamic interaction, and Brownian motion are the most important influences. The properties of the suspension are strongly depending on the balance of the microscopic forces between the particles. Especially for industrial processes, where one needs to optimize certain material properties a detailed understanding of the relevant influences is needed. The stability of different microstructures and especially the clustering process are key properties which are

of interest.

In our work we investigate these properties, focusing on  $\text{Al}_2\text{O}_3$  particles of diameter  $0.37\text{ }\mu\text{m}$  suspended in water. This is a widely used material in ceramics [20, 21]. We have developed a simulation code for a Brownian suspension [22] and have adjusted the simulation parameters so that the simulation corresponds quantitatively to a real suspension such that experimental data can be compared directly. The diffusion coefficient, sedimentation velocity [22], and the viscosity of the suspension can be reproduced [23]. We also have tested the influence of polydispersity and found that its influence on the results is small. It is much more important to choose the correct mean size of the particles [23]. For  $\text{Al}_2\text{O}_3$  suspensions attractive van der Waals forces are important for the behavior of this material. Electrostatic repulsion of the charged particles counteracts the attraction and can prevent clustering depending on the particle surface charge. In Ref. [23] we have presented how one can relate parameters of DLVO potentials [7, 8] with experimental conditions. In the experiment one can control the pH-value and the salt concentration. The latter can be expressed by the ionic strength  $I$ , which is an effective concentration of all ions present in the solution. Both, the pH-value and the ionic strength, influence the charge of the colloidal particles. We have shown that for not too strongly attractive forces one can obtain reasonable quantitative agreement with experimental results: by adjusting the lubrication force, which represents the short range hydrodynamics, we are able to reproduce rheological data of a real suspension [23].

Three regimes can be identified and plotted in a stability diagram [23], which we want to investigate here in more detail: A clustered regime, in which particles aggregate to clusters, a fluid-like and stable suspension and a repulsive region, for which the microstructure is similar to the ones known from glassy systems. From our previous work we know that our model works well, even quantitatively, in the suspended regime of the stability diagram and close to the borders between the different microstructures. In this paper we extend our investigations to different  $pH$ -values, deeper in the clustered regime, and to the repulsive structure. We expect to gain insight to the microscopic structure on a qualitative level.

On these grounds we have explored the stability diagram of  $Al_2O_3$  suspensions. The particles are uncharged close to the so called “isoelectric point” at  $pH = 8.7$ . There, for all ionic strengths the particles form clusters. For lower  $pH$ -values particles can be stabilized in solution, because they are charged. For low  $pH$ -values, low salt concentrations, and high volume fractions a repulsive structure can be found.

In the following section we shortly describe our simulation method. After that we discuss the criteria we apply to characterize the microstructures. We utilize the pair correlation function and the structure factor to characterize the clustering behavior. Both of them in principle contain the same information, but we concentrate on certain peaks in either of them. Each peak in the correlation function and in the structure factor corresponds to a certain length scale and we chose either the correlation function or the structure factor, depending on which of the two quantities is more suitable under numerical criterions to observe on a given length scale. In the section thereafter we describe our simulation setup. In the results section we start with the discussion of the correlation function and the structure factor. Additionally, we evaluate the so-called demixing parameter  $\Psi$  [24]. To characterize the repulsive region we evaluate the mean squared displacement (MSD), which shows a plateau, if the particle motion consists of different processes acting on well separated time scales. Finally, the results are summarized in a stability diagram for our  $Al_2O_3$ -suspension. It shows the behavior of the suspension in an intuitive way and helps to design industrial processes using this material.

## II. SIMULATION METHOD

Our simulation method consists of two parts: a Molecular Dynamics (MD) code, which treats the colloidal particles, and a Stochastic Rotation Dynamics (SRD) simulation for the fluid solvent.

In the MD part of our simulation the colloidal particles are represented by monodisperse spheres. We include effective electrostatic interactions and van der Waals attraction, known as DLVO potentials [7, 8], a lubrication force and Hertzian contact forces. DLVO potentials are composed of two terms, the first one being an exponentially screened Coulomb potential due to the surface charge of the suspended particles

$$V_{\text{Coul}} = \pi \varepsilon_r \varepsilon_0 \left[ \frac{2 + \kappa d}{1 + \kappa d} \cdot \frac{4 k_B T}{ze} \tanh \left( \frac{ze \zeta}{4 k_B T} \right) \right]^2 \times \frac{d^2}{r} \exp(-\kappa[r - d]), \quad (1)$$

where  $d$  denotes the particle diameter and  $r$  is the distance between the particle centers.  $e$  is the elementary charge,  $T$  the temperature,  $k_B$  the Boltzmann constant, and  $z$  is the valency of the ions of added salt.  $\varepsilon_0$  is the permittivity of the vacuum,  $\varepsilon_r = 81$  the relative dielectric constant of the solvent.  $\kappa$  is the inverse Debye length defined by  $\kappa^2 = 8\pi \ell_B I$ , with the ionic strength  $I$  and the Bjerrum length  $\ell_B = 7 \text{ \AA}$ . The first fraction in Eq. (1) is a correction to the DLVO potential (in the form used in Ref. [25]), which takes the surface curvature into account and is valid for spherical particles [26].

The effective surface potential  $\zeta$  is the electrostatic potential at the border between the diffuse layer and the compact layer. Smoluchowski related it to the electrokinetic mobility of the particle as  $\mu = \zeta \varepsilon_0 \varepsilon_r / \eta$  [27]. The  $\zeta$  potential can be related to the  $pH$ -value of the solvent with a so-called  $2pK$  charge regulation model [23].

The Coulomb term competes with the second part of the DLVO potential which is given by the attractive van der Waals interaction

$$V_{\text{vdW}} = -\frac{A_H}{12} \left[ \frac{d^2}{r^2 - d^2} + \frac{d^2}{r^2} + 2 \ln \left( \frac{r^2 - d^2}{r^2} \right) \right]. \quad (2)$$

$A_H = 4.76 \cdot 10^{-20} \text{ J}$  is the Hamaker constant [25]. The DLVO potentials exhibit two minima, one primary minimum, where the particles touch each other. Eq. (2) diverges where in reality the primary minimum of the potential is located. Therefore we model the primary minimum by cutting off the DLVO potentials for small separations and substituting them

by a parabola which is connected in continuously differentiable manner to the DLVO potential. This cutoff is made at distances of several nanometers, where the potential has already reached negative values, i.e. where the potential decends to the primary minimum. The primary minimum is separated by a potential barrier from the secondary minimum, which occurs at larger particle distances and which is less deep. For low salt concentrations, i.e., large Debye screening lengths, the electrostatic repulsion overcompensates the van der Waals attraction and the secondary minimum disappears.

Long range hydrodynamic interactions are taken into account in the simulation for the fluid as described below. This can only reproduce interactions correctly down to a certain length scale. On shorter distances, a lubrication force has to be introduced explicitly in the Molecular Dynamics simulation:

$$\mathbf{F}_{\text{lub}} = -\mathbf{v}_{\text{rel},\perp} \frac{6\pi\eta}{r-d} \left(\frac{d}{4}\right)^2, \quad (3)$$

with the relative velocity  $\mathbf{v}_{\text{rel},\perp}$  projected on the connecting line of the particle centers.  $\eta$  is the dynamic viscosity of the fluid. Our implementation of the interaction contains cutoff radii to connect it to the long-range hydrodynamics and to avoid numerical instability for particles touching each other [22, 23].

To avoid that the particles penetrate each other, we are using a Hertz force described by the potential

$$V_{\text{Hertz}} = K(d-r)^{5/2} \quad \text{if } r < d, \quad (4)$$

where  $K$  is an interaction constant and additionally a damping term

$$\mathbf{F}_{\text{Damp}} = -\mathbf{v}_{\text{rel},\perp} \beta \sqrt{d-r}, \quad (5)$$

with a damping constant  $\beta$ . For the integration of the translational motion we utilize a velocity Verlet algorithm [28].

For the simulation of a fluid solvent, many different simulation methods have been proposed: Stokesian Dynamics (SD) [3, 29, 30], Accelerated Stokesian Dynamics (ASD) [31, 32], pair drag simulations [4], Brownian Dynamics (BD) [25, 33], Lattice Boltzmann (LB) [1, 2, 34, 35], and Stochastic Rotation Dynamics (SRD) [22, 36, 37]. These mesoscopic fluid simulation methods have in common that they make certain approximations to reduce the computational effort. Some of them include thermal noise intrinsically, or it can be included consistently. They scale differently with the number of embedded particles and the complexity of the algorithm differs largely.

We apply the Stochastic Rotation Dynamics method (SRD) introduced by Malevanets and Kapral [38, 39]. It intrinsically contains fluctuations, is easy to implement, and has been shown to be well suitable for simulations of colloidal and polymer suspensions [22, 23, 36, 37, 40, 41, 42] and very recently for star-polymers in shear flow [43]. The method is also known as “Real-coded Lattice Gas” [36] or as “multi-particle-collision dynamics” (MPCD) [44]. It is based on so-called fluid particles with continuous positions and velocities. A streaming step and an interaction step are performed alternately. In the streaming step, each particle  $i$  is moved according to

$$\mathbf{r}_i(t+\tau) = \mathbf{r}_i(t) + \tau \mathbf{v}_i(t), \quad (6)$$

where  $\mathbf{r}_i(t)$  denotes the position of the particle  $i$  at time  $t$  and  $\tau$  is the time step. In the interaction step the fluid particles are sorted into cubic cells of a regular lattice and only the particles within the same cell interact among each other according to an artificial interaction. The interaction step is designed to exchange momentum among the particles, but at the same time to conserve total energy and total momentum within each cell, and to be very simple, i.e., computationally cheap: each cell  $j$  is treated independently. First, the mean velocity  $\mathbf{u}_j(t') = \frac{1}{N_j(t')} \sum_{i=1}^{N_j(t')} \mathbf{v}_i(t)$  is calculated.  $N_j(t')$  is the number of fluid particles contained in cell  $j$  at time  $t' = t + \tau$ . Then, the velocities of each fluid particle in cell  $j$  are rotated according to

$$\mathbf{v}_i(t+\tau) = \mathbf{u}_j(t') + \mathbf{\Omega}_j(t') \cdot [\mathbf{v}_i(t) - \mathbf{u}_j(t')]. \quad (7)$$

$\mathbf{\Omega}_j(t')$  is a rotation matrix, which is independently chosen at random for each time step and each cell. We use rotations about one of the coordinate axes by an angle  $\pm\alpha$ , with  $\alpha$  fixed. The coordinate axis as well as the sign of the rotation are chosen at random, resulting in 6 possible rotation matrices. To remove anomalies introduced by the regular grid, one can either choose a mean free path of the order of the cell size or shift the whole grid by a random vector once per SRD time step as proposed by Ihle and Kroll [45, 46].

Three different methods to couple the SRD and the MD simulation have been introduced in the literature. Inoue *et al.* proposed a way to implement no slip boundary conditions on the particle surface [36]. Padding and Louis very recently came up with full slip boundaries, where the fluid particles interact via Lennard-Jones potentials with the colloidal particles [47]. Falck *et al.* [48] have developed a

“more coarse grained” method which we use for the simulations of the present paper and which we describe shortly in the following.

To couple the colloidal particles to the fluid, the colloidal particles are sorted into the SRD cells and their velocities are included in the rotation step. One has to use the mass of each particle—colloidal or fluid particle—as a weight factor when calculating the mean velocity

$$\mathbf{u}_j(t') = \frac{1}{M_j(t')} \sum_{i=1}^{N_j(t')} \mathbf{v}_i(t) m_i, \quad (8)$$

$$\text{with} \quad M_j(t') = \sum_{i=1}^{N_j(t')} m_i, \quad (9)$$

where we sum over all colloidal and fluid particles in the cell, so that  $N_j(t')$  is the total number of both particles, fluid plus colloidal ones.  $m_k$  is the mass of the particle with index  $i$  and  $M_j(t')$  gives the total mass contained in cell  $j$  at time  $t' = t + \tau$ . In summary, the algorithm for the fluid simulation is described by Eqns. (6)–(9). To some of our simulations we apply shear. This is realized by explicitly setting the mean velocity  $\mathbf{u}_j$  to the shear velocity in the cells close to the border of the system. Both, colloidal and fluid particles, are involved in this additional step. A thermostat is applied to remove the energy introduced to the system by the shear force. We have described the simulation method in more detail in Refs. [22, 23].

### III. BACKGROUND

In this paper we examine the microstructures obtained in our simulations for different conditions. We vary the  $pH$ -value and the ionic strength  $I$ . The shear rate  $\dot{\gamma}$  as an external influence is varied as well. We classify the microstructures in three categories: suspended, clustered, and repulsive. In the suspended case, the particles can move freely in the fluid and do not form stable clusters. In the clustered regime the particles form clusters due to attractive van der Waals forces. These clusters can be teared apart if shear is applied. In some of our simulations the clusters are very weakly connected and at small shear rates they are not only broken up into smaller pieces, but they dissolve to freely moving individual particles. In this case, we assign the microstructure to the suspended region, although in complete absence of the shear flow clusters are formed. At the borders between the different regimes in fact no sharp transitions can be observed. The DLVO forces rather steadily increase and compete with the

hydrodynamic interactions. Accordingly, in experiments one cannot observe a sudden solidification, but a steadily increasing viscosity when leaving the suspended regime [23].

Similarly as for attractive forces, repulsive interactions can restrict the mobility of the particles. If this happens, the mean squared displacement of the particles shows a pronounced plateau, as it can be found in glassy systems. However, we speak of a “repulsive structure”, because the change of the viscosity is not as strong as in glasses, where it often changes by many orders of magnitude, when the glass transition is approached. In addition, to claim a system shows a glassy behavior would require to investigate the temperature dependence of a typical time (e.g. particle diffusion time) and to show its divergence as the glass temperature is approached. This is difficult to do in the framework of our simulation model [22] and therefore we prefer to speak about a “repulsive structure” which might be identified as a colloidal glass in future work.

In this paper we would like to emphasize the analysis of the microstructure for different conditions. Our aim is to reproduce a so-called stability diagram by simulations. The stability diagram depicts the respective microstructure depending on the  $pH$ -value and the ionic strength  $I$ . We apply different numerical tools to analyze the microstructure in our simulations and finally arrive at a stability diagram shown in Fig. 10, which summarizes the results which we present in the following sections.

The first tool we apply for that is the pair correlation function

$$g(r) = \frac{V}{N^2} \left\langle \sum_i \sum_{j \neq i} \delta(r - r_{ij}) \right\rangle, \quad (10)$$

(see Ref. [28] p.55), where  $V$  is the volume,  $N$  the number of particles and  $r_{ij}$  the distance of two particles  $i$  and  $j$ , can be used for a first characterization of the system. It shows maxima at certain typical particle distances, e.g. there is a nearest neighbor peak, and more complicated structures at larger distances, which we have assigned to typical particle configurations for small distances [22]. Here, we use the next-neighbor-peak to analyze our data, which provides information of the short-range structure of the suspension. To observe the long-range structure we move on to its complementary quantity: the structure factor, defined by

$$S(\mathbf{k}) = \frac{1}{N} \sum_{l,m=1}^N \exp(i\mathbf{k} \cdot \mathbf{r}_{lm}), \quad (11)$$

where  $N$  is the number of particles, and  $\mathbf{r}_{lm}$  is the vector from particle  $l$  to particle  $m$ .  $i$  denotes the imaginary unit here. The structure factor is defined in  $\mathbf{k}$ -space and it is related to the pair correlation function in real space by a three dimensional Fourier transform:

$$S(k) - 1 = \int d\mathbf{r} \exp(i\mathbf{k} \cdot \mathbf{r}) \rho g(r), \quad (12)$$

with the density  $\rho$ . Therefore, in principle the structure factor contains the same information as the pair correlation function. However, due to numerical reasons and our implementation of shear boundary conditions it is easier to observe the long-range structure in the structure factor than in the pair correlation function. For our evaluation it is important that in a finite system  $\mathbf{k}$ -vectors are restricted to discrete vectors  $2\pi \left( \frac{n_x}{L_x}, \frac{n_y}{L_y}, \frac{n_z}{L_z} \right)$  with  $L_{x,y,z}$  being the system size in  $x$ -,  $y$ -, and  $z$ -direction and  $n_{x,y,z} \in \mathbb{Z}$ . We evaluate  $S(\mathbf{k})$  for these  $\mathbf{k}$ -vectors and use  $|S(\mathbf{k})|$  for further analysis. Since we do not evaluate the anisotropy of the structure factor in this study, we average over all possible orientations of the  $\mathbf{k}$ -vector. We sort the absolute values of the  $\mathbf{k}$ -vectors into intervals and average within these intervals over the values of the structure factors. Let us now discuss some typical features of the structure factor, corresponding to typical length scales present in the system.

One typical length for dense systems is about one particle diameter, the distance particle centers have to keep so that they do not overlap. The corresponding peak of the structure factor is the nearest neighbor peak at  $k = \frac{2\pi}{d}$ . In a single crystal the peak would be sharp, since the particle positions are well defined, whereas in our case of a suspension there is a certain disorder, which broadens the peak.

Similar to the nearest neighbor peak another peak can be detected at twice the  $\mathbf{k}$ -vector, which corresponds to a distance of one particle radius. This does not necessarily mean that there are particles whose centers are only one particle radius apart. It only means that for a certain  $\mathbf{k}$ -vector the addends in Eq. (11) do not cancel out each other.

For small  $\mathbf{k}$ -vectors there is another peak, or in our case an increase of the structure factor towards low  $\mathbf{k}$ -vectors. The length scale corresponds to the size of the whole system. If large clusters are formed, this can be seen in an increase of the low- $\mathbf{k}$ -peak, since the contributions on this length scale do not cancel out each other anymore.

As already mentioned, later in this paper we focus on the low- $\mathbf{k}$ -peak which corresponds to

a length scale of the size of the system.

#### IV. SIMULATION SETUP

In this study the colloidal particles are represented by three dimensional spheres of  $d = 0.37 \mu\text{m}$  in diameter. This is the mean diameter of the particles used in the experiments to which we refer in Ref. [23]. We have simulated a small volume,  $24d = 8.88 \mu\text{m}$  long in  $x$ -direction, which is the shear direction, and  $12d = 4.44 \mu\text{m}$  long in  $y$ - and  $z$ -direction. We have varied the volume fraction between  $\Phi = 10\%$  (660 particles) and  $\Phi = 40\%$  (2640 particles). Most of the simulations were performed at  $\Phi = 35\%$  (2310 particles). We use periodic boundaries in  $x$ - and  $y$ -direction and closed boundaries in  $z$ -direction [23]. Shear is applied in  $x$ -direction by moving small zones of particles and fluid close to the wall with a given shear velocity. The  $xy$ -plane is our shear plane. For simulations without shear, to achieve the best comparability, we use the same boundary conditions and just set the shear rate to  $\dot{\gamma} = 0$ . In addition we have performed simulations with two different shear rates: with  $\dot{\gamma} = 100/\text{s}$  and with  $\dot{\gamma} = 500/\text{s}$ . For better comparability to other works the Peclet number

$$Pe = 6\pi\eta R^3\dot{\gamma}/k_B T, \quad (13)$$

which expresses the importance of Brownian motion with respect to the shear flow, is useful. The Peclet numbers in our shear simulations are  $Pe = 3$  and  $Pe = 15$ , respectively.

#### V. RESULTS AND DISCUSSION

First, we focus on simulations without shear, where one can predict intuitively, what should happen. Qualitatively the results are similar to our earlier work [22], but the quantitative relation between the  $pH$ -value and the potentials is new. The relation was presented in Ref. [23], but here we apply it to different cases and we focus more on the characterization of the microstructure. However, given the particle particle interaction potentials, the microstructure in equilibrium can be predicted easily, at least on a qualitative level. But, the matter changes and gets more sophisticated, when shear is applied and an interplay between shear flow and particle particle interactions becomes responsible for the resulting microstructure.

### A. Correlation function

For constant ionic strength  $I = 3 \text{ mmol/l}$  the local microstructure can be examined using the correlation function. Depending on the  $pH$ -value the behavior of the system changes from a repulsive structure around  $pH = 4$  to a stable suspension around  $pH = 6$  towards a clustered region if the  $pH$ -value is further increased, until the isoelectric point is reached at  $pH = 8.7$ . There clustering occurs in any case, independent on the ionic strength. This can be seen in the structure of the correlation function: electrostatic repulsion prevents clustering (at  $pH = 4$ ). Particles are suspended, and there is no fixed long range ordering in the system. The correlation function (Fig. 1) shows a maximum at a typical nearest neighbor distance slightly above  $\frac{r}{d} = 1$  with  $d$  denoting the particle diameter, then in the layer of next neighbors small correlations can be found (at  $\frac{r}{d} = 2$ ). For larger distances the correlation function is rather constant.

When the  $pH$ -value is increased, the surface charge is lower, which at first causes the particles to approach each other more closely. The maximum of the correlation function is shifted to smaller distances (see Fig. 1, note that the curves are shifted vertically in the plot by a factor of 3 for better visibility.). Then, van der Waals attraction becomes more important and clustering begins. One can see this in the correlation function where a sharp structure at particle distances between 1.5 and 2 particle diameters occurs. In a solid like cluster the position of the next neighbor is fixed more sharply than in the suspension, consequently the nearest neighbor peak becomes sharper, too, and its height is increased. Close to the isoelectric point ( $pH = 8.7$ ) the barrier between primary and secondary minimum disappears. The particles, once clustered, cannot rearrange anymore, and therefore the correlations to the next neighbors become less sharp again (compare the cases of  $pH = 8.7$  and  $pH = 7.7$  in Fig. 1 at the positions denoted by the arrows).

Instead of varying the  $pH$ -value, one can also vary the ionic strength to achieve similar effects. Increasing the ionic strength, experimentally speaking “adding salt” decreases the screening length  $1/\kappa$  and therefore the attractive forces become more important: the particles start to form clusters. On the contrary, if the ionic strength is decreased—experimentally speaking a dialysis step is performed—the electrostatic repulsion prevents cluster formation and, for sufficiently strong repulsion, long range correlations occur as soon as the range of the

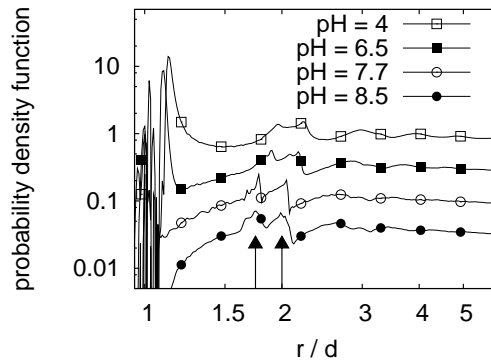


Figure 1: Dependence of the particle correlation function on the  $pH$  value,  $I = 3 \text{ mmol/l}$ ,  $\dot{\gamma} = 0/\text{s}$ ,  $\Phi = 35\%$ . The plots for four different  $pH$ -values are shifted against each other for better visibility by a factor of 3. For  $pH = 4$  the particles are not clustered. Hence the structure at  $\frac{r}{d} = 2$  is less sharp than in the other three curves of the plot and the nearest neighbor peak (at  $\frac{r}{d} = 1$ ) is broad. For  $pH = 6.5$  slight clustering starts, the structures become sharper. For  $pH = 7.7$  strong cluster formation is reflected in very sharp structures. For  $pH = 8.5$  electrostatic repulsion nearly disappears so that no barrier between primary and secondary minimum exists anymore. The particles cannot rearrange anymore, and therefore the structures labeled by the arrows become smoothed compared to the case of  $pH = 7.7$ .

repulsion reaches the mean particle distance.

In Fig. 2 one can see clustering in the primary minimum of the potential as well as in the very shallow secondary minimum. The correlation function plotted there is evaluated after 1000 SRD time steps in a simulation for  $pH = 7$  and  $I = 3 \text{ mmol/l}$  at a volume fraction of  $\Phi = 35\%$  sheared with  $\dot{\gamma} = 100/\text{s}$ . Note that the shear flow is not of essential importance here, but it supports the particles to overcome the potential barrier between the primary and the secondary minimum. The dotted lines in Fig. 2 denote the zero line.

A secondary minimum only exists if the screening length of the electrostatic repulsion is short enough, i.e., if the ionic strength is large enough. According to the depth of the potential, clustering in the primary minimum is associated with much stronger forces than in the secondary minimum.

The effects described up to here can be observed with or without shear qualitatively in an analogous manner. If the suspension is sheared clustering occurs at higher  $pH$ -values and the peaks found in the correlation function are slightly broadened, because the relative particle positions are less fixed. But a new fea-

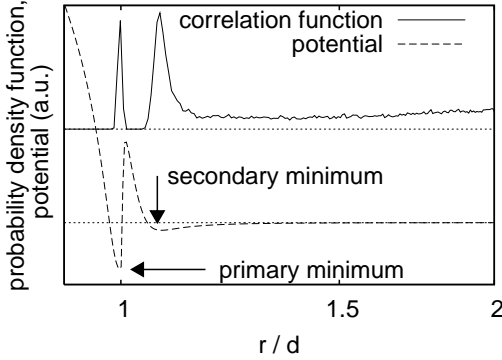


Figure 2: Correlation function,  $\dot{\gamma} = 100/\text{s}$ ,  $pH = 7$ ,  $I = 3 \text{ mmol/l}$ ,  $\Phi = 35\%$ : one finds clustering in the primary and the secondary minimum. Note: The vertical axis is logarithmic, and a constant offset has been added before plotting. Thereby, the coincidence of the minima in the potential with the maxima in the correlation function becomes more apparent. The dotted lines denote the position of the base line before shifting.

ture appears, if a stable suspension of not too high volume fraction is sheared. Induced by the shear particles arrange themselves in layers. Regular nearest neighbor distances in the shear plane cause the correlation function to become more structured even for large distances (see Fig. 3). The long range structure of the pair correlation function appears after a transient time the particles need to arrange themselves in the layered structure. The curves in Fig. 3 correspond to the same simulation, but for increasing time from bottom to top. The arrows from the bottom indicate the position of the next-neighbor peak and the next but one neighbors (Since the particles do not touch each other, the peaks are located not exactly at  $\frac{r}{d} = 1, 2, 3, \dots$ ). Within one layer which moves as a whole, a hexagonal particle order appears, which can be seen in the occurrence of a peak at  $\frac{r}{d} = \sqrt{3}$  times the position of the nearest neighbor peak, i.e., the next neighbor peak splits, as indicated by the arrows from above. The same applies to the next but one neighbor peak marked by the second set of arrows at  $3 < r/d < 4$ . Shear induced layer formation has been found in both, experiments [49, 50] and simulations [51, 52, 53]

We have integrated over the nearest neighbor peaks, both, the peaks of the primary and the secondary minimum, and plotted the integral versus  $pH$ -value in Fig. 4. We have chosen  $I = 3 \text{ mmol/l}$  and  $\Phi = 35\%$  and three different shear rates:  $\dot{\gamma} = 0, 100$  and  $500/\text{s}$ . We have integrated the correlation function for

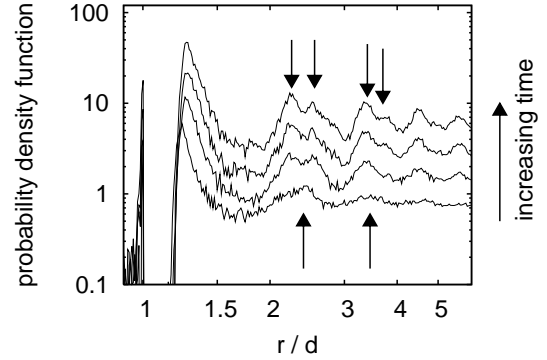


Figure 3: Correlation function for  $\dot{\gamma} = 500/\text{s}$ ,  $pH = 6$ ,  $I = 0.3 \text{ mmol/l}$ ,  $\Phi = 32\%$ : depending on the simulation time the peaks indicated by the arrows from below split into two (indicated by the arrows from above), and long range correlations occur (for  $\frac{r}{d} > 4$ ). This reflects the process of layer formation and appearing of a regular (hexagonal) order in the layers. From bottom to top several states for increasing time are shown. The plots are shifted vertically by a factor of 2 for better visibility.

$r < 1.215d$ , where for all  $pH$ -values the potential in the secondary minimum has a value of  $-\frac{1}{2}k_B T$ . In other words, we have captured the primary and the secondary minimum of the potential for this plot. For low  $pH$ -values clustering (in the secondary minimum) is only possible for low shear rates. For high shear rates, the hydrodynamic forces do not allow the formation of stable clusters. For rising  $pH$ -values the clustering increases, first for the un-sheared suspension, at higher  $pH$ -values for low shear rates ( $\dot{\gamma} = 100/\text{s}$ ) and finally for high shear rates ( $\dot{\gamma} = 500/\text{s}$ ). Remarkably, for  $pH > 7.5$  the curve for  $\dot{\gamma} = 100/\text{s}$  shows stronger cluster formation than the other ones. Particles are brought together by the shear flow, so that compared to the case of no shear, the clustering process is supported here. On the other hand, the shear stress may not be too strong, because otherwise the clustering process is limited by the shear flow again (for  $\dot{\gamma} = 500/\text{s}$  the clustering is less pronounced than for  $\dot{\gamma} = 100/\text{s}$ ).

## B. Structure Factor

The pair correlation function can be used to characterize the local order of the microstructure on the length scale of the particle size. However, to do the characterization on the length scale of the system size, we use the structure factor  $S(\mathbf{k})$ . In principle we could integrate the correlation function  $g(r)$  over an interval for

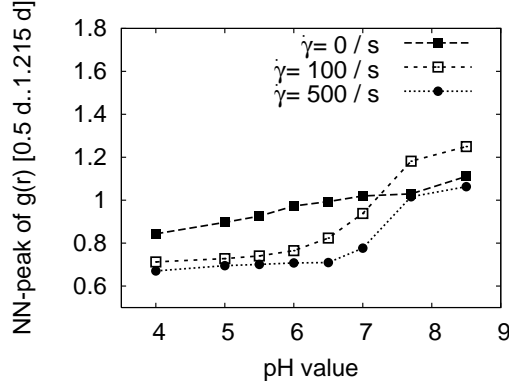


Figure 4: Nearest neighbor peak (primary and secondary minimum of the potential) of the correlation function  $I = 3 \text{ mmol/l}$ ,  $\Phi = 35\%$ : For low  $pH$ -values clustering is prevented by the electrostatic repulsion. For high  $pH$ -values the particles form clusters, which is reflected by an increased nearest neighbor peak. First, shear prevents clustering, then depending on the shear rate, cluster formation takes place. Low shear rates even support cluster formation at high  $pH$ -values.

large  $r$ . However, due to our implementation of shear (see Ref. [23]), we have to close the boundary in  $z$ -direction. Therefore we already find restrictions for  $r$  around half the extension of the system in this direction. We find that it is easier to handle these finite size restrictions by moving on to the structure factor. There, we always find a low- $\mathbf{k}$ -peak, even if no cluster formation takes place in the simulation. In contrast to experiments, where this peak only appears for clustered samples, it reflects the presence of a typical length of the system size in the simulation. Namely, the finite size of the simulation volume is the typical length, which appears in the structure factor by the low- $\mathbf{k}$ -peak. This only produces a constant offset when integrating over the low- $\mathbf{k}$ -peak as we are going to do below in this section. Thus, it is easy to handle the influence of the finite system size in  $\mathbf{k}$ -space.

In Fig. 5 we have plotted several typical structure factors of our simulations. For these plots the  $pH$ -value is fixed to  $pH = 6$ . The cases a) and b) are sheared with  $\dot{\gamma} = 500/\text{s}$  at an ionic strength of  $I = 0.3 \text{ mmol/l}$ . In case a) the volume fraction  $\Phi = 20\%$  is relatively low. Therefore the particles can arrange themselves in layers parallel to the shear plane, which move relatively independently in the shear flow. They have a certain distance fixed in space and time. This can be seen in a sharp peak at a dimensionless  $\mathbf{k}$ -vector of  $k = 5.2$ , which corresponds to a distance of 1.2 particle diameters. In fact, this is exactly the distance between two neighboring

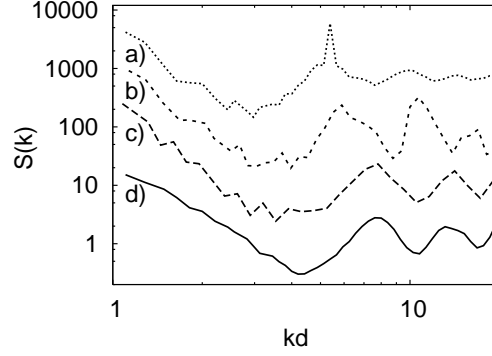


Figure 5: Structure factor for some selected examples, with  $pH = 6$  fixed for all plots:  $\dot{\gamma} = 500/\text{s}$ ,  $I = 0.3 \text{ mmol/l}$ : a)  $\Phi = 20\%$  and b)  $\Phi = 35\%$ ,  $\dot{\gamma} = 0$ ,  $I = 25 \text{ mmol/l}$ : c)  $\Phi = 40\%$  and d)  $\Phi = 10\%$ . The curves are shifted vertically for better visibility. In case a) ten layers can be identified in the system, resulting in the strong peak close to 5. But, since the particles in the layers can still move freely, there is no  $2^{\text{nd}}$ -order-peak. In case b) layers are formed, but particles are moving from one layer to the other, disturbing the flow. As a result the nearest neighbor peak is much broader. Due to the structure in the layers, a  $2^{\text{nd}}$ -order-peak appears. In case c) the interaction is strongly attractive, hence the particles approach each other and the nearest neighbor peak is shifted to higher  $\mathbf{k}$ -vectors. In case d) the volume fraction is much less. The slope of the low- $\mathbf{k}$ -peak is much flatter, which depicts that the cluster is fractal.

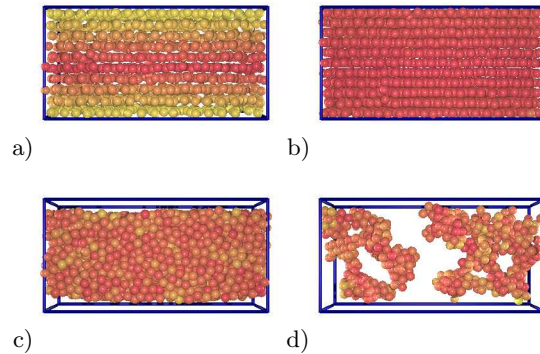


Figure 6: (Color online) Snapshots of the systems analyzed in Fig. 5: In case a) one can see the layers resulting in the sharp peak in the structure factor. In case b) the layers are packed closer due to the higher volume fraction. Collisions between particles of neighboring layers happen more frequently. In case c) one big cluster is formed. The particles are packed densely. In case d) the fractal nature of the system can be seen directly.



layers, as one can easily verify by counting the layers in a snapshot of the system (Fig. 6a)). The particles in the layers do not have a fixed distance and therefore no  $2^{nd}$ -order-peak can be observed.

For case b) the volume fraction is increased to  $\Phi = 35\%$ . The particle layers are packed more densely and therefore the interactions between one layer and the neighboring one become relevant. Particles jump from one layer to the other, which disturbs the flow and therefore the distance between the layers is not fixed anymore. The sharp peak on top of the nearest neighbor peak disappears. Instead of that, in each layer a regular hexagonal order appears and therefore the  $2^{nd}$ -order-peak is much more pronounced.

In case c) the ionic strength is increased to  $I = 25$  mmol/l. The inter-particle potentials are attractive enough that aggregation takes place. In this simulation we did not apply shear, therefore one finds only one big cluster in the system (compare Fig. 6c)). In the cluster the particles are packed more densely and consistently the nearest neighbor peak in the structure factor is shifted to larger  $\mathbf{k}$ -vectors. The volume fraction is  $\Phi = 40\%$  in this case.

In case d) the volume fraction is decreased to  $\Phi = 10\%$ . The particles still form clusters, but their mobility is not high enough to create one compact cluster. The system has a fractal structure (see Fig. 6d)). This can be seen in the structure factor as well: The slope of the low- $\mathbf{k}$ -peak is flatter in this case compared to cases a)–c). A flatter slope of the low- $\mathbf{k}$ -peak is typical for structure factors of fractal objects. The fractal dimension of the cluster extracted from the slope of the low- $\mathbf{k}$ -peak is 2.5. In experiments this relation is often used to determine the fractal dimension of a sample: Latuada et al. [54] have evaluated the fractal dimension of agglomerates of latex particles from the slope of the structure factor. McCarthy et al. [55] give an introduction to scattering intensities at fractal objects, without mentioning the structure factor, but their arguments refer to the contribution of the structure factor on the scattering intensity. The underlying mechanism which is responsible for these structures is cluster cluster aggregation[56].

In Fig. 7 we show the dependence of the low- $\mathbf{k}$ -peak of the structure factor on the  $pH$ -value. Here we have integrated over dimensionless  $\mathbf{k}$ -vectors smaller than 3 which means, we have captured structures larger than twice a particle diameter. A large integral over the low- $\mathbf{k}$ -peak is due to a large inhomogeneity in the system. In one part of the system parti-

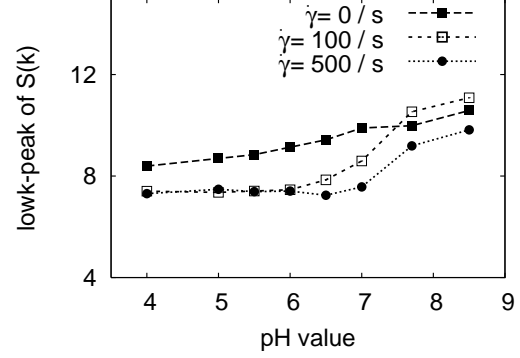


Figure 7: low- $\mathbf{k}$ -peak for different  $pH$ -values and different shear rates. The ionic strength  $I$  is kept constant at  $I = 3$  mmol/l and the volume fraction is always  $\Phi = 35\%$ . For  $\dot{\gamma} = 0$ /s the particles tend to cluster in the secondary minimum of the potential. This clustering can easily be broken up, if shear is applied. If the  $pH$ -value is increased, shear cannot prevent cluster formation anymore. At low shear rates ( $\dot{\gamma} = 100$ /s) clustering is even enhanced, since the particles are brought closer to each other by the shear flow. Note that the offset of the plots reflects the finite size of our system combined with the closed boundary conditions (see the text).

cles are present and in the other part not. In other words, we observe the process of cluster formation on a length scale of the system size. Without shear, particles cluster in the secondary minimum for all  $pH$ -values. If the system is slightly sheared ( $\dot{\gamma} = 100$ /s) clustering is suppressed for low  $pH$ -values. Starting at  $pH = 6$  cluster formation starts and is even supported by the shear flow for  $pH$ -values larger than 7.5. For large shear rates ( $\dot{\gamma} = 500$ /s) cluster formation is suppressed by the shear flow. By analyzing the low- $\mathbf{k}$ -peak of the structure factor one observes on the length scale of the system size. The same behavior of the system can be seen by analyzing the pair correlation function, as we have already shown in Fig. 4. In that case one analyzes the number of nearest neighbors, that means, one observes the length scale of a particle diameter. Nevertheless, both graphs show the same behavior of the system, i.e., we have a consistent picture of the cluster formation process on the length scale of the nearest neighbors and on the length scale of the system size.

Thus we have confirmed that the cluster formation process is not limited to length scales smaller than our system size. This is reflected especially by the transition between  $pH = 7 - 8$  and its shear rate dependence in the plots in Fig. 7 and Fig. 4. There is a strong similarity of the two plots, which are obtained by two evalu-

ation methods referring to two different length scales. This confirms that the plots do not only reflect how clusters are formed on the respective length scale, but that the clustering process is a phenomenon which can be observed on *any* length scale by applying a suitable method to characterize it.

### C. Density Inhomogeneity

Another way to observe the cluster formation process is provided by the “demixing parameter” defined in Ref. [24] as follows: the system is divided into  $n^3$  cubes and the particle density  $\rho_k$  is evaluated in each cube. Then the demixing parameter is the mean squared deviation of the density

$$\Psi_n = \sum_{k=0}^{n^3} (\rho_k - \bar{\rho})^2, \quad (14)$$

where  $\bar{\rho}$  is the mean density. For our elongated system we modify this definition and use  $2n$  cubes in  $x$ -direction, resulting in  $2n^3$  cubes in total. The demixing parameter implicitly contains information about the density of the clusters. It is the density fluctuation of the whole system. If the clusters are more compact, voids have to appear and the demixing parameter increases, since the distribution of the local density is broadened thereby.

In Fig. 8 we have plotted the demixing parameter  $\Psi_4$  versus time for three different shear rates and four different ionic strengths in each plot. The  $pH$ -value is kept constant at  $pH = 6$  and the volume fraction at  $\Phi = 35\%$ . Without shear  $\Psi_4$  is nearly constant. Even if a cluster is formed, it does not move, so that the average density in the boxes does not change much. For lower volume fractions the time dependence without shear is stronger. If shear is applied the clusters are deformed so that stronger inhomogeneities appear. Depending on the ionic strength the demixing parameter increases with cluster formation (high ionic strength) or still stays constant when the interactions are repulsive (low ionic strength). For  $\dot{\gamma} = 100/s$  the strongest cluster formation is achieved for the highest ionic strength  $I = 20 \text{ mmol/l}$ . If the ionic strength is decreased, the clustering effect decreases as well, until it disappears completely at  $I = 1 \text{ mmol/l}$ , where the repulsive regime is reached. To see the shear rate dependence, compare the plots for  $\dot{\gamma} = 100/s$  and  $500/s$ . If the shear rate is increased, the cluster formation starts faster because the shear flow brings

the particles faster in contact, but the resulting inhomogeneity of the final state is less than for lower shear rates. This effect can be seen in Fig. 4 and Fig. 7, too. There, also the intensity of the respective peaks for  $\dot{\gamma} = 500/s$  is less than for  $\dot{\gamma} = 100/s$ . This shows again that large shear rates can inhibit cluster formation, whereas moderate shear rates can support the clustering process (the plots in Fig. 8 b) for  $\dot{\gamma} = 100/s$  are steeper than the ones in Fig. 8 a) for  $\dot{\gamma} = 0/s$ .) In addition to the information already contained in other quantities we have presented, Fig. 8 shows the time evolution. One can see three regimes of time evolution: for very short times all plots are nearly constant. This means that the cluster formation has not yet started. Then, the plots for attractive potentials raise, which shows the onset of cluster formation. For large times the slope of the plots decreases, which reflects that the clusters have been formed and no more “demixing” takes place. Without shear (see Fig. 8 a)), it is remarkable that for the largest ionic strength the growth of the demixing parameter first becomes constant after 0.3 s, whereas for the other cases where clustering occurs, it grows further. This reflects that in the case of  $I = 20 \text{ mmol/l}$  the attraction is that strong that no reordering of the particles is possible anymore.

### D. Repulsive Regime

To characterize the repulsive regime, we evaluate the mean squared displacement for the particles. In Fig. 9 we plot the mean squared displacement for different ionic strengths. The  $pH$ -value is kept constant at  $pH = 6$  and the volume fraction is  $\Phi = 35\%$  for this plot. Three different regimes can be identified. For very short times, the ballistic regime: particles move on short distances without a notable influence by their neighbors. The distances are in the order of some percent of the particle diameter and the times are a few SRD time steps. For larger times the particles interact with their neighbors and therefore their mobility is limited due to collisions with the neighbors. This is reflected in the mean squared displacement by a plateau of reduced slope, which is the more pronounced the more the mobility of the particles is restricted. For even larger time scales collective motion starts, i.e., clusters or groups of particles move, or single particles can escape from a cage formed by its neighbors. Depending on the ionic strength different effects are important and thus the shape of the curve is different. For large ionic strengths the particles

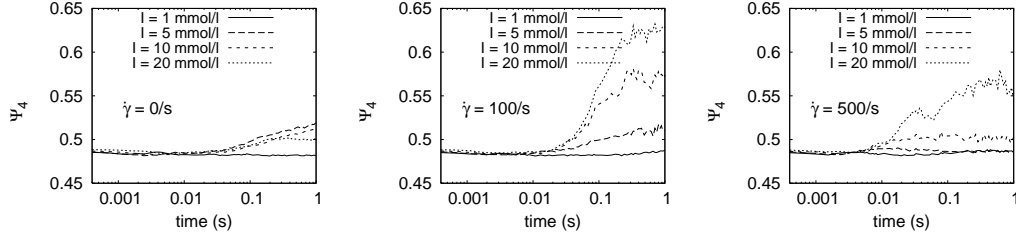


Figure 8: Demixing parameter for constant  $pH = 6$  and volume fraction  $\Phi = 35\%$  for three different shear rates:  $\dot{\gamma} = 0/s$  (left),  $100/s$  (center) and  $500/s$  (right). Without shear only very weak demixing takes place. For  $\dot{\gamma} = 100/s$  the strongest demixing can be observed for the system with the highest ionic strength  $I = 20\text{ mmol/l}$ . For lower ionic strengths the effect decreases until it disappears completely at  $I = 1\text{ mmol/l}$ , where the repulsive regime is reached. If the shear rate is further increased ( $\dot{\gamma} = 500/s$ ), the clusters are less stable so that the system becomes less inhomogeneous. For  $I = 5\text{ mmol/l}$  the demixing is even suppressed completely.

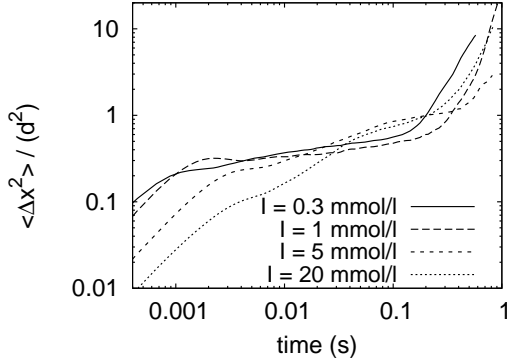


Figure 9: Mean squared displacement at  $pH = 6$  for different ionic strengths, without shear. One can see a ballistic regime for short times, a central plateau and a collective long time movement which can be a movement of a whole cluster or cage escape events of single particles. Depending on the ionic strength, the central plateau is more or less pronounced. A comparison of the plateau for different simulations can be used to decide, if a certain state belongs to the repulsive region of the stability diagram. A state well in the liquid microstructure should be used as a reference for the comparison.

form clusters and these clusters may drift or rotate in the system. Then the collective motion is more dominant and the mean squared displacement grows faster than in single particle diffusion. The mean squared displacement does not show a plateau, then. But in the repulsive regime, the neighbors limit the motion of the particles, and the slope of the plateau is flatter, i.e., the plateau is even more pronounced, compared to the suspended case. In the repulsive regime the particles tend to arrange themselves in layers when shear is applied [23] and long range correlations can be found in un-sheared systems [22].

## E. Stability Diagram

The results of the investigations presented in this paper can be summarized in a stability diagram for our  $\text{Al}_2\text{O}_3$ -suspension (Fig. 10). Three different microstructures can be identified: a repulsive structure, a suspended region and a clustered region. In contrast to our previous work [22, 23], we have explored the parameter space more in the repulsive regime and deeper in the clustered region. We use the mean squared displacement, the demixing parameter  $\Psi$  [24], the correlation function, and the structure factor, to decide to which of the three microstructures a certain point in the stability diagram belongs. However, the borders between the regions are not sharp and they depend on the shear rate. We have indicated the crossover regions by the shaded patterns in the stability diagram. If the volume fraction is decreased, the region of the repulsive structure becomes smaller.

To decide if a state is in the suspended region or in the repulsive one of the stability diagram, we have compared the plots of the mean squared displacement for the simulations without shear. If the plateau was pronounced there, we have counted the state among the repulsive regime. As a second criterion one can compare the pair correlation function. If there are long range correlations even though the system is not sheared, then the microstructure is the repulsive one. Finally, the shear force can be used to localize the border to the repulsive regime. For a given shear rate and a fixed volume fraction, the shear force depends on the particle interactions. If the shear force increases compared to a state well in the suspended regime, the motion of the particles is blocked by the electrostatic interaction in the repulsive regime.

As we have mentioned in Sec.III, without

shear weak clustering can be seen in the suspended case as well, since there is no barrier for the particles to enter the secondary minimum of the DLVO potential, but the clusters can be broken up again very easily. Thus, to decide, if a state belongs to the clustered or to the suspended regime, we first study the snapshots of the system. If we see no clusters there, the clustered regime can be excluded. But, if we see clusters, we next check the density of the clusters and the onset time of the increase of the demixing parameter  $\Psi$ , which is a measure for the time it takes to form clusters. Both, the density and the time are indications for the stability of the clusters. If they grow slowly and their density is low, we count the state to the suspended regime. The demixing parameter  $\Psi$  shown in Fig. 8 implicitly contains information about the density of the clusters. It is the density fluctuation of the whole system. If the clusters are more compact, voids have to appear and the demixing parameter increases, since the distribution of the local density is broadened thereby. The stability diagram obtained by these criteria is consistent with the results of the simulations with shear flow, shown in Fig. 4 and Fig. 7. Especially, the increased cluster formation for  $I = 3 \text{ mmol/l}$  starting between  $\text{pH} = 7 - 8$  is reflected in an increased nearest neighbor peak in Fig. 4, and low- $\mathbf{k}$ -peak in Fig. 7 respectively, and in a border between suspended and clustered regime in Fig. 10. The repulsive structure for  $\text{pH} = 4$  and  $I = 3 \text{ mmol/l}$  can not be recognized in Fig. 4 and Fig. 7, but in a pronounced layer formation.

## VI. SUMMARY AND OUTLOOK

We have simulated colloidal particles in shear flow and investigated how the clustering process due to attractive DLVO potentials is affected by the hydrodynamic forces. We find a consistent behavior on different length scales. The nearest neighbor peak of the pair correlation function has been used to observe the direct neighborhood of the particles and the low- $\mathbf{k}$ -peak of the structure factor to keep track of the length scales up to the system size. In both cases a suppression of the cluster formation by the shear flow can be seen at low  $\text{pH}$ -values. For large  $\text{pH}$ -values low shear rates even support the clustering process. In contrast, for high shear rates it suppresses the cluster formation. We have evaluated the mean squared displacement and the demixing parameter  $\Psi$  [24] in order to draw the stability dia-

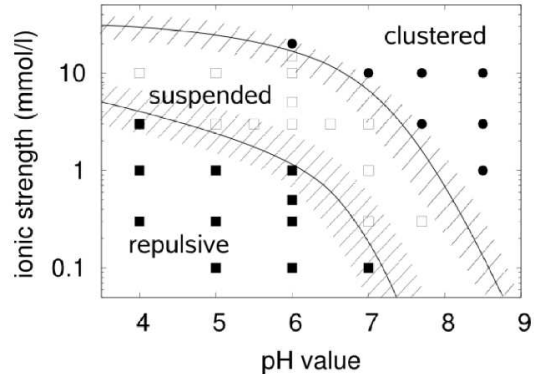


Figure 10: Stability diagram (plotted for  $\Phi = 35\%$  and without shear): depicting three regions: a clustered region (filled circles), a suspended regime (open squares), and a repulsive structure (filled squares). In the clustered region particles aggregate which leads to inhomogeneity in the system. In the suspended regime, the particles are distributed homogeneously in the system and they can move freely. In the repulsive regime the mobility of the particles is restricted by electrostatic repulsion exerted by their neighbors. As a result they arrange in a local order which maximizes nearest neighbor distances. The borders between the regimes are not sharp. They depend on the shear rate and on the volume fraction. Therefore we have indicated the crossover regions by the shaded patterns. The lines are guides to the eye.

gram as given in Fig. 10. To our knowledge this stability diagram for  $\text{Al}_2\text{O}_3$  suspensions is reproduced quantitatively for the first time from simulations. It helps to predict the behavior of a real suspension. Our findings on the cluster formation process suggest that soft stirring can enhance the cluster formation in industrial processing of this material. Further investigations can be carried out on the fractal dimension and its dependence on the experimental conditions. The low- $\mathbf{k}$ -peak of the structure factor can be used for that. The cluster size distribution could as well deliver interesting insights useful to design industrial processes. Apart from that one can apply our algorithm to different materials. To do so, one has to change the interaction constants and especially for the electrostatic repulsion the calibration we have presented in Ref. [23] are necessary. We expect that the stability diagram does not change qualitatively, but the position of the borders will be different.

### Acknowledgments

This work has been financed by the German Research Foundation (DFG) within the project DFG-FOR 371 “Peloide”. We thank G. Gudehus, G. Huber, M. Külzer, L. Harnau, M. Bier, J. Reinshagen, and S. Richter for valuable collaboration.

This work is resulting in large parts from the collaboration with the group of A. Coniglio,

Università di Napoli “Federico II”, Naples, Italy. M. Hecht thanks him and his group for his hospitality and for the valuable support during his stay there. M. Hecht thanks the DAAD for the scholarship (Doktorandenstipendium) which enabled him the stay.

The computations were performed on the IBM p690 cluster at the Forschungszentrum Jülich, Germany and at HLRS, Stuttgart, Germany.

- 
- [1] A. J. C. Ladd. Numerical simulations of particulate suspensions via a discretized Boltzmann equation. part 1. theoretical foundation. *J. Fluid Mech.*, 271:285–309, 1994.
  - [2] A. J. C. Ladd. Numerical simulations of particulate suspensions via a discretized Boltzmann equation. part 2. numerical results. *J. Fluid Mech.*, 271:311–339, 1994.
  - [3] T. N. Phung, J. F. Brady, and G. Bossis. Stokesian dynamics simulation of Brownian suspensions. *J. Fluid Mech.*, 313:181–207, 1996.
  - [4] L. E. Silbert, J. R. Melrose, and R. C. Ball. Colloidal microdynamics: Pair-drag simulations of model-concentrated aggregated systems. *Phys. Rev. E*, 56(6):7067–7077, December 1997.
  - [5] K. Geoffrey Soga, John R. Melrose, and Robin C. Ball. Metastable states and the kinetics of colloid phase separation. *J. Chem. Phys.*, 110(4):2280–2288, 1999.
  - [6] L. Harnau and S. Dietrich. Depletion potential in colloidal mixtures of hard spheres and platelets. *Phys. Rev. E*, 69:051501, 2004.
  - [7] E. J. W. Verwey and J. T. G. Overbeek. *Theory of the Stability of Lyophobic Colloids*. Elsevier, Amsterdam, 1948.
  - [8] B. V. Derjaguin and L. D. Landau. Theory of the stability of strongly charged lyophobic sols and of the adhesion of strongly charged particles in solutions of electrolytes. *Acta Physicochimica USSR*, 14:633, 1941.
  - [9] S. Alexander, P. M. Chaikin, P. Grant, G. J. Morales, P. Pincus, and D. Hone. Charge renormalization, osmotic pressure, and bulk modulus of colloidal crystals: Theory. *J. Chem. Phys.*, 80(11):5776–81, 1984.
  - [10] M. J. Grimson and M. Silbert. A self-consistent theory of the effective interactions in charge-stabilized colloidal dispersions. *Macromol. Phys.*, 74(2):397–404, 1991.
  - [11] René van Roij and J.-P. Hansen. Van der Waals-like instability in suspensions of mutually repelling charged colloids. *Phys. Rev. Lett.*, 79(16):3082–85, 1997.
  - [12] J. Dobnikar, Y. Chen, R. Rzehak, and H. H. von Grünberg. Many-body interactions in colloidal suspensions. *J. Phys.: Condens. Matter*, 15:S263, 2003.
  - [13] V. Trappe, V. Prasad, L. Cipelletti, P. N. Segre, and D. A. Weitz. Jamming phase diagram for attractive particles. *Nature*, 411(3):772–774, 2001.
  - [14] Y. Levin, T. Trizac, and L. Bocquet. On the fluid-fluid phase separation in charged-stabilized colloidal suspensions. *J. Phys.: Condens. Matter*, 15:S3523, 2003.
  - [15] A.-P. Hynninen, M. Dijkstra, and R. van Roij. Effect of three-body interactions on the phase behavior of charge-stabilized colloidal suspensions. *Phys. Rev. E*, 69:061407, 2004.
  - [16] A. de Candia, E. del Gado, A. Fierro, N. Sator, and A. Coniglio. Colloidal gelation, percolation and structural arrest. *Physica A*, 358:239–248, 2005.
  - [17] J. Dobnikar, R. Rzehak, and H. H. von Grünberg. Effect of many-body interactions on the solid-liquid phase behavior of charge-stabilized colloidal suspensions. *Europhys. Lett.*, 61(5):695–701, 2003.
  - [18] T. Palberg, W. Mönch, F. Bitzer, R. Piazza, and T. Bellini. Freezing transition for colloids with adjustable charge: A test of charge renormalization. *Phys. Rev. Lett.*, 74:4555, 1995.
  - [19] R. Yamamoto, K. Kim, Y. Nakayama, K. Miyazaki, and D. R. Reichman. On the role of hydrodynamic interactions in colloidal gelation. *arXiv:cond-mat/0604404*, 2006.
  - [20] R. Oberacker, J. Reinshagen, H. von Both, and M. J. Hoffmann. Ceramic slurries with bimodal particle size distributions: Rheology, suspension structure and behavior during pressure filtration. In N. Claussen S. Hirano, G.L. Messing, editor, *Ceramic Processing Science VI*, volume 112, pages 179–184. American Ceramic Society, Westerville, OH (USA), 2001. ISBN 1574981048.
  - [21] J. Reinshagen, R. C. D. Cruz, R. Oberacker, and J. Hoffmann. Electrostatically stabilized alumina suspensions with defined interparticle potentials: I. influence of salt concentration on suspension conductivity and rheology. 2006. (to be submitted).
  - [22] Martin Hecht, Jens Harting, Thomas Ihle, and Hans J. Herrmann. Simulation of claylike colloids. *Phys. Rev. E*, 72:011408, jul 2005.

- [23] Martin Hecht, Jens Harting, Markus Bier, Jörg Reinshagen, and Hans J. Herrmann. Shear viscosity of clay-like colloids in computer simulations and experiments. *Phys. Rev. E*, 74:021403, 2006.
- [24] A. M. Puertas, M. Fuchs, and M. E. Cates. Simulation study of nonergodicity transitions: Gelation in colloidal systems with short-range attractions. *Phys. Rev. E*, 67:031406, 2003.
- [25] M. Hütter. *Brownian Dynamics Simulation of Stable and of Coagulating Colloids in Aqueous Suspension*. PhD thesis, Swiss Federal Institute of Technology Zurich, 1999.
- [26] L. Bocquet, E. Trizac, and M. Aubouy. Effective charge saturation in colloidal suspensions. *J. Chem. Phys.*, 117:8138, 2002.
- [27] M. Smoluchowski. Contribution à la théorie de l'endosmose électrique et de quelques phénomènes corrélatifs. *Bulletin International de l'Académie des Sciences de Cracovie*, 8:182–200, 1903.
- [28] M. P. Allen and D. J. Tildesley. *Computer simulation of liquids*. Oxford Science Publications. Clarendon Press, Oxford, 1987.
- [29] J. F. Brady and G. Bossis. Stokesian dynamics. *Ann. Rev. Fluid Mech.*, 20:111–57, 1988.
- [30] J. F. Brady. The rheological behavior of concentrated colloidal suspensions. *J. Chem. Phys.*, 99(1):567–81, 1993.
- [31] A. Sierou and J. F. Brady. Accelerated stokesian dynamics simulations. *J. Fluid Mech.*, 448:115, 2001.
- [32] A. Sierou and J. F. Brady. Shear-induced self-diffusion in non-colloidal suspensions. *J. Fluid Mech.*, 506:285, 2004.
- [33] M. Hütter. Local structure evolution in particle network formation studied by brownian dynamics simulation. *J. Colloid Interface Sci.*, 231:337–350, 2000.
- [34] A. J. C. Ladd and R. Verberg. Lattice-boltzmann simulations of particle-fluid suspensions. *J. Stat. Phys.*, 104(5):1191, 2001.
- [35] A. Komnik, J. Harting, and H. J. Herrmann. Transport phenomena and structuring in shear flow of suspensions near solid walls. *Journal of Statistical Mechanics: theory and experiment*, P12003, 2004.
- [36] Y. Inoue, Y. Chen, and H. Ohashi. Development of a simulation model for solid objects suspended in a fluctuating fluid. *J. Stat. Phys.*, 107(1):85–100, 2002.
- [37] J. T. Padding and A. A. Louis. Hydrodynamic and brownian fluctuations in sedimenting suspensions. *Phys. Rev. Lett.*, 93:220601, 2004.
- [38] A. Malevanets and R. Kapral. Mesoscopic model for solvent dynamics. *J. Chem. Phys.*, 110:8605, 1999.
- [39] A. Malevanets and R. Kapral. Solute molecular dynamics in a mesoscale solvent. *J. Chem. Phys.*, 112:7260, 2000.
- [40] M. Ripoll, K. Mussawisade, R. G. Winkler, and G. Gompper. Low-reynolds-number hydrodynamics of complex fluids by multi-particle-collision dynamics. *Europhys. Lett.*, 68:106–12, 2004.
- [41] R. G. Winkler, K. Mussawisade, M. Ripoll, and G. Gompper. Rod-like colloids and polymers in shear flow: a multi-particle-collision dynamics study. *J. Phys.: Condens. Matter*, 16(38):S3941–54, 2004.
- [42] I. Ali, D. Marenduzzo, and J. M. Yeomans. Dynamics of polymer packaging. *J. Chem. Phys.*, 121:8635–8641, November 2004.
- [43] M. Ripoll, R. G. Winkler, and G. Gompper. Star polymers in shear flow. *Phys. Rev. Lett.*, 96:188302, 2006.
- [44] M. Ripoll, K. Mussawisade, R. G. Winkler, and G. Gompper. Dynamic regimes of fluids simulated by multiparticle-collision dynamics. *Phys. Rev. E*, 72:016701, 2005.
- [45] T. Ihle and D. M. Kroll. Stochastic rotation dynamics I: Formalism, galilean invariance, green-kubo relations. *Phys. Rev. E*, 67(6):066705, 2003.
- [46] T. Ihle and D. M. Kroll. Stochastic rotation dynamics II: Transport coefficients, numerics, long time tails. *Phys. Rev. E*, 67(6):066706, 2003.
- [47] J. T. Padding and A. A. Louis. Hydrodynamic interactions and brownian forces in colloidal suspensions: Coarse-graining over time and length-scales. *Phys. Rev. E*, 74:031402, 2006.
- [48] E. Falck, J. M. Lahtinen, I. Vattulainen, and T. Ala-Nissila. Influence of hydrodynamics on many-particle diffusion in 2d colloidal suspensions. *Eur. Phys. J. E*, 13:267–275, 2004.
- [49] B. J. Ackerson and P. N. Pusey. Shear-induced order in suspensions of hard spheres. *Phys. Rev. Lett.*, 61(8):1033, 1988.
- [50] B. J. Ackerson, C. G. DeKruif, N. J. Wagner, and W. B. Russel. Comparison of small shear flow rate-small wave vector static structure factor data with theory. *J. Chem. Phys.*, 90(6):3250, 1989.
- [51] J. R. Melrose and D. M. Heyes. Simulations of electrorheological and particle mixture suspensions: Agglomerate and layer structures. *J. Chem. Phys.*, 98(7):5873–5886, 1993.
- [52] Alan A. Catherall, John R. Melrose, and Robin C. Ball. Shear thickening and order-disorder effects in concentrated colloids at high shear rates. *Journal of Rheology*, 44(1):1–25, 2000.
- [53] I. Cohen, T. G. Mason, and D. A. Weitz. Shear-induced configurations of confined colloidal suspensions. *Phys. Rev. Lett.*, 93(4):046001, 2004.
- [54] M. Lattuada, H. Wu, and M. Morbidelli. Estimation of fractal dimension of colloidal gels in the presence of multiple scattering. *Phys. Rev. E*, 64:061404, 2001.
- [55] D. W. McCarthy, J. E. Mark, and D. W. Schaefer. Synthesis, structure, and properties of hybrid organic-inorganic composites based on polysiloxanes. i. poly(dimethylsiloxane) elastomers containing silica. *J. Polym. Sci. B*, 36(7):1167, 1998.

- [56] K. Geoffrey Soga, John R. Melrose, and Robin C. Ball. Continuum percolation and depletion flocculation. *J. Chem. Phys.*, 108(14):6026–6032, 1998.